
This is an electronic reprint of the original article.
This reprint may differ from the original in pagination and typographic detail.

Sun, Kewei; Kurki, Lauri; Silveira, Orlando J.; Nishiuchi, Tomohiko; Kubo, Takashi; Foster, Adam S.; Kawai, Shigeki

On-Surface Synthesis of Silole and Disila-Cyclooctene Derivatives

Published in:
Angewandte Chemie - International Edition

DOI:
[10.1002/anie.202401027](https://doi.org/10.1002/anie.202401027)

Published: 24/04/2024

Document Version
Publisher's PDF, also known as Version of record

Published under the following license:
CC BY

Please cite the original version:
Sun, K., Kurki, L., Silveira, O. J., Nishiuchi, T., Kubo, T., Foster, A. S., & Kawai, S. (2024). On-Surface Synthesis of Silole and Disila-Cyclooctene Derivatives. *Angewandte Chemie - International Edition*, 63(18), Article e202401027. <https://doi.org/10.1002/anie.202401027>

This material is protected by copyright and other intellectual property rights, and duplication or sale of all or part of any of the repository collections is not permitted, except that material may be duplicated by you for your research use or educational purposes in electronic or print form. You must obtain permission for any other use. Electronic or print copies may not be offered, whether for sale or otherwise to anyone who is not an authorised user.

VIP On-Surface Synthesis Very Important Paper

 How to cite: *Angew. Chem. Int. Ed.* **2024**, *63*, e202401027
 doi.org/10.1002/anie.202401027

On-Surface Synthesis of Silole and Disila-Cyclooctene Derivatives

 Kewei Sun,* Lauri Kurki, Orlando J. Silveira, Tomohiko Nishiuchi, Takashi Kubo,
 Adam S. Foster,* and Shigeki Kawai*


Abstract: The incorporation of Si atoms into organic compounds significantly increases a variety of functionality, facilitating further applications. Recently, on-surface synthesis was introduced into organosilicon chemistry as 1,4-disilabenzene bridged nanostructures were obtained via coupling between silicon atoms and brominated phenyl groups at the ortho position on Au(111). Here, we demonstrate a high generality of this strategy via syntheses of silole derivatives and nano-ribbon structures with eight-membered sila-cyclic rings from dibrominated molecules at the *bay* and *peri* positions on Au(111), respectively. Their structures and electronic properties were investigated by a combination of scanning tunneling microscopy/spectroscopy and density functional theory calculations. This work demonstrates a great potential to deal with heavy group 14 elements in on-surface silicon chemistry.

Introduction

Organosilicon chemistry deals with syntheses and characterization of compounds containing carbon-silicon (C–Si) bonds. Ever since the first synthesis of tetraethylsilane by Friedel and Crafts in 1863,^[1,2] various synthetic strategies have been developed for the molecules with C–Si bonds, such as silyl ethers,^[3] silyl chlorides,^[4] silenes^[5] and siloles.^[6] Among them, the silicon incorporated cyclic ring, namely sila-cyclic ring, has attracted the attention of researchers and

engineers^[6–9] because the sila-cyclic ring can be used for various applications such as catalysis,^[10,11] precursors of molecular transformation,^[12,13] electron transport^[14,15] and light-emitting materials.^[16,17] Although several sila-cyclic rings have been synthesized,^[6–9] it remains highly important to explore new reactions and synthesize novel sila-cyclic ring structures.

On-surface chemistry deals with the important study of chemical reactions and characterization of molecules on solid substrates. In the reaction, small organic molecules adsorbed on metal surfaces are usually activated by annealing,^[18,19] irradiated light,^[20,21] and injected tunneling electrons^[22,23] and subsequently conjugated with each other. The advantage of on-surface synthesis relates to the high-controllability of the structures, which can be defined by the employed precursor molecules.^[24] So far, various surface reactions have been demonstrated, such as Ullmann-type coupling,^[18,22,25] Glaser-type coupling,^[26–28] Bergman-type reaction,^[29,30] Sonogashira-type coupling,^[31–33] and dehydrogenated coupling.^[34,35] Very recently, C–Si bond coupling was obtained by reacting bromo-substituted molecules to Si atoms directly on Au(111), leading to the formation of 1,4-disilabenzene bridged covalent organic frameworks (COFs) and graphene nanoribbons (GNRs).^[36] This strategy is expected to have a high generality for the synthesis of multiple sila-cyclic rings with appropriate precursors.

Here, we demonstrate the on-surface synthesis of five and eight-membered sila-cyclic rings on Au(111). 2,2',6,6'-tetrabromobiphenyl **1** having two bromines (Br) at the *bay* position reacted with Si atoms to form two siloles (C₄Si) incorporated into a molecule at 420 K. For 1,4,5,8-tetrabro-

[*] Dr. K. Sun

 International Center for Young Scientists
 National Institute for Materials Science
 1-2-1 Sengen, Tsukuba, Ibaraki 305-0047 (Japan)
 E-mail: SUN.Kewei@nims.go.jp

 Dr. L. Kurki, Dr. O. J. Silveira, Prof. Dr. A. S. Foster
 Department of Applied Physics
 Aalto University
 P.O. Box 11100, Aalto, Espoo 00076 (Finland)
 E-mail: adam.foster@aalto.fi

 Prof. Dr. T. Nishiuchi, Prof. Dr. T. Kubo
 Department of Chemistry, Graduate School of Science
 Osaka University,
 Toyonaka 560-0043 (Japan)

 Prof. Dr. A. S. Foster
 Nano Life Science Institute (WPI-NanoLSI)
 Kanazawa University
 Kakuma-machi, Kanazawa 920-1192 (Japan)

Prof. Dr. S. Kawai

 Center for Basic Research on Materials
 National Institute for Materials Science
 1-2-1 Sengen, Tsukuba, Ibaraki 305-0047 (Japan)
 E-mail: KAWAI.Shigeki@nims.go.jp

 Prof. Dr. S. Kawai
 Graduate School of Pure and Applied Sciences,
 University of Tsukuba,
 Tsukuba 305-8571 (Japan)

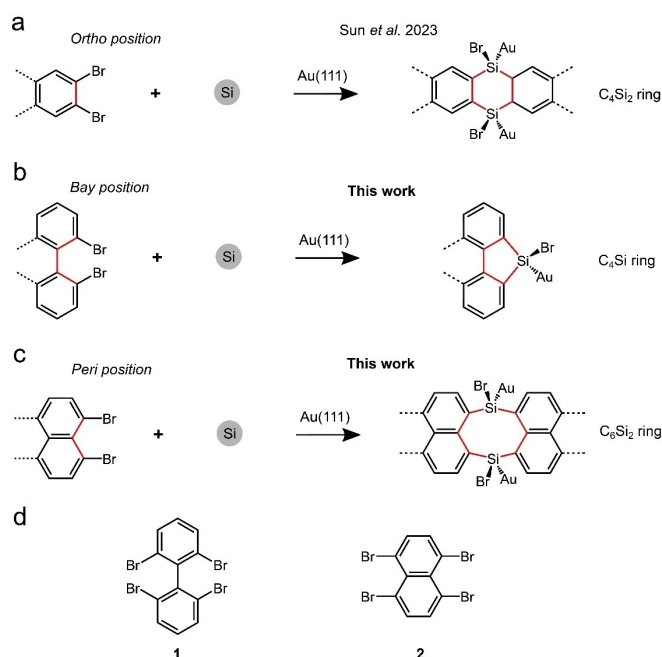
© 2024 The Authors. Angewandte Chemie International Edition published by Wiley-VCH GmbH. This is an open access article under the terms of the Creative Commons Attribution License, which permits use, distribution and reproduction in any medium, provided the original work is properly cited.

monaphthalene **2** having two Br at the *peri* position, corrugated nanoribbon structures embedded with eight-membered sila-cyclic rings (C_6Si_2) were generated by reacting with Si atoms after annealing at 470 K. Each Si atom in the cyclic rings was passivated by one Br atom, which was then removed by high-temperature annealing. The structure and the electronic properties of the products were investigated with a combination of scanning tunneling microscopy/spectroscopy (STM/STS) and density functional theory (DFT) calculations.

Results and Discussion

In our previous study, two Br atoms at *ortho* position of peripheral phenyl groups in 2,3,6,7,10,11-hexabromotriphenylene reacted to Si atoms adsorbed on Au(111), yielding 1,4-disilabenzene (C_4Si_2 ring) bridged nanostructures (Scheme 1a).^[36] Following this concept, two Br atoms at *bay* (Scheme 1b) and *peri* positions (Scheme 1c) are used for syntheses of five-membered sila-cyclic ring (C_4Si) and eight-membered sila-cyclic ring (C_6Si_2) by conjugating **1** and **2** with Si atoms on Au(111), respectively (Scheme 1d).

We first deposited Si atoms on a clean Au(111) surface and subsequently annealed the substrate at 420 K to form the $AuSi_x$ submonolayer (Figure S1).^[36–38] After depositing **1** on the surface kept at room temperature, the sample was heated at 420 K for 5 min. Small clusters indicated by arrows



Scheme 1. On-surface reactions between bromo-substituted aromatic hydrocarbons and Si atoms on Au(111). Two Br atoms at (a) *ortho* position of phenyl group: synthesis of 1,4-disilabenzene (C_4Si_2) bridged nanostructures (previous work);^[36] (b) *bay* position of biphenyl group: synthesis of five-membered ring (C_4Si); (c) *peri* position of naphthyl group: synthesis of eight-membered ring (C_6Si_2) bridged structures. (d) **1** and **2** as precursors.

in Figure 1a correspond to silicon bromide $SiBr_x$ ($x=1, 2, 3, 4$) molecules, which is in agreement with our previous work.^[39] Among them, $SiBr_4$ molecule is highly volatile and can desorb from the Au(111) surface even at room temperature in vacuum. Thus, the partially covered $AuSi_x$ layer acts as a source of Si atoms for on-surface reaction.^[36] We also found isolated molecules with two bright dots marked by dashed squares. Since such features are absent in the on-surface synthesis only with **1** on Au(111) (Figure S2). We found three different types of products (Figure 1a). Among them, Type 1 has the highest chemoselectivity of 86% (Figure S3). The close-up view shows two bright dots at both right- and left-hand sides of the molecule (Figure 1b). To investigate the inner structure, the STM tip apex was terminated by a CO molecule.^[40,41] The high-resolution constant height dI/dV map (Figure 1c, Figure S4) and the corresponding Laplace filtered image (Figure 1d) show the biphenyl backbone at the middle and two sets of five-membered rings at both sides. Thus, debrominated **1** was connected to two Si atoms, resulting in formation of silole rings (Figure 1e). We also found each Si atom was terminated by one Br that appeared as a bright dot (Figure 1b). A similar reaction at the *ortho* position was observed in the formation of 1,4-disilabenzene.^[36] Our DFT electron density of the Type 1 deposited on a bare Au(111) surface showed that the silicon atoms adsorb on top positions and bond significantly with the substrate gold atoms, slightly buckling the molecule due to an elevation of the bromine atoms (Figure 1f). We also performed STM and dI/dV simulations which confirmed that the sharp line appearing near the C–Si bond (Figure 1d) is not a direct observation of the chemical bond, but it is rather caused by mechanical bending of the functionalized CO tip (Figure 1h). The C–Si bond length was 1.90 Å which is a typical length for a C–Si single bond.^[42] The structures of Type 2 and Type 3 were also investigated with bond-resolved STM. Type 2 is longer than Type 1 in length (Figure 1i). The corresponding bond-resolved image shows that the structure is composed of biphenyl groups and two silole rings (Figure 1j, Figure S5). We assume that the molecular units are connected to each other via a Si–Si bond (Figure 1k), which is further illustrated by DFT simulation (inset of Figure 1j, Figure S6). The slight left-right asymmetry observed in Type 2 structures (Figure 1j) may relate to either the different adsorption heights due to the different adsorption sites or the asymmetric CO-tip. Type 3 corresponds to the single unit, yet one Br seems to be replaced by one hydrogen atom (Figure S7), which may originate from the substrate and/or residual gas in the vacuum chamber.^[43] After annealing at a higher temperature (520 K), most molecules form the disordered nanostructures (Figure S8).

Next, the electronic properties of Type 1 were measured by STS (Figure 2a). The differential conductance dI/dV spectra were recorded at four different sites of Type 1 and one site on the bare Au(111) surface for the reference as indicated by dots in the inset of Figure 2a. Besides the Au surface state appearing around -0.5 V, two characteristic peaks at -0.6 V and 2.5 V with respect to the Fermi level were identified as the highest occupied molecular orbital

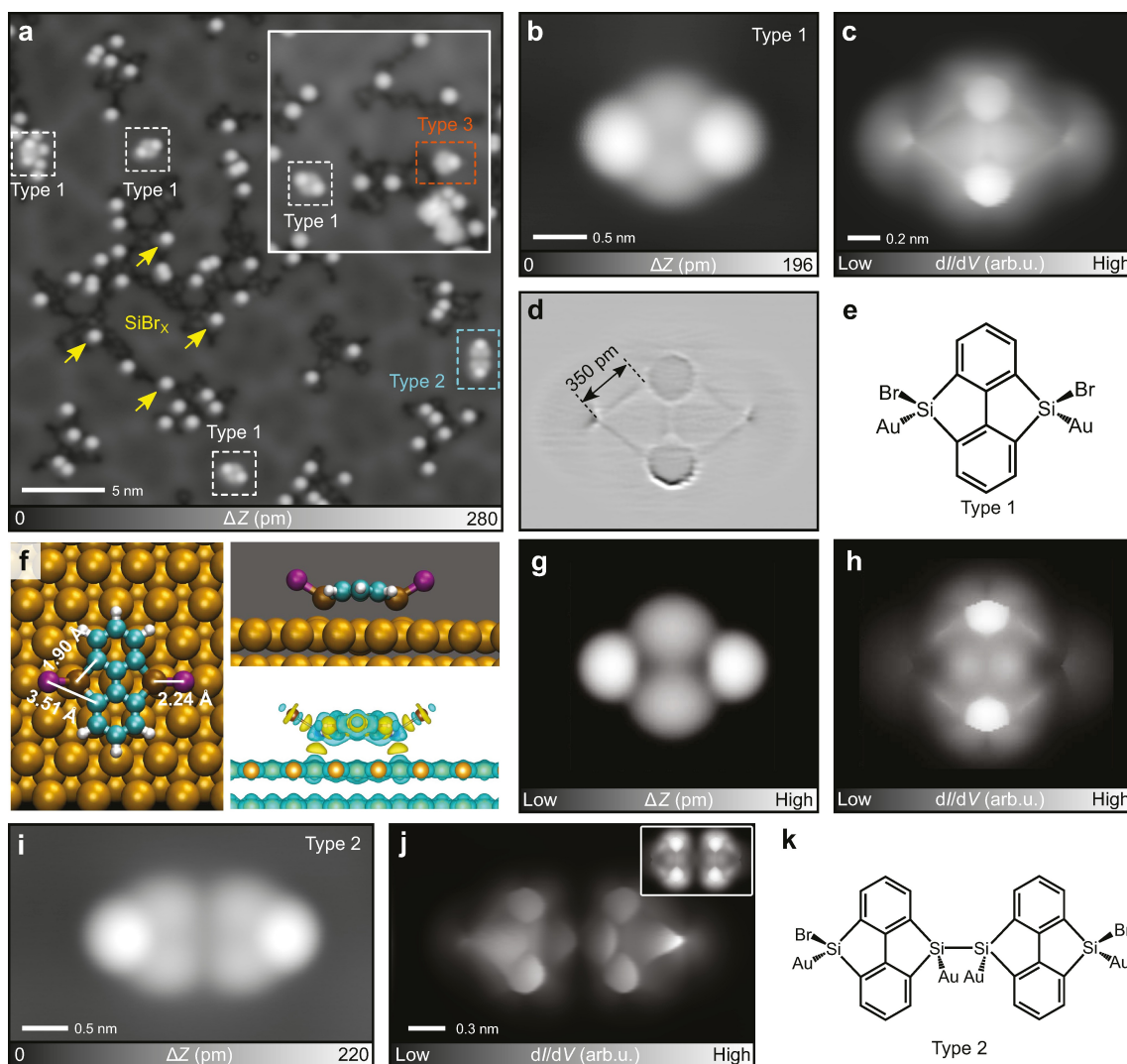


Figure 1. Synthesis of five-membered sila-cyclic rings from **1** on Au(111). (a) STM topography of Type 1 and Type 2 molecules as well as SiBr_x clusters obtained by annealing at 420 K for 5 min. The inset shows Type 3 found in another area. (b) Close-up view of Type 1, (c) the bond-resolved dI/dV map, and (d) the corresponding Laplace filtered image. (e) Chemical structure of Type 1. (f) Top (left) and side view (right-top) of DFT optimized structure of Type 1 on Au(111) and the electron density difference (right-bottom), (g) simulated STM image, and (h) simulated bond-resolved image. (i) Close-up view of Type 2 and (j) the corresponding constant height dI/dV map. The inset shows the simulated bond-resolved image. (k) Chemical structure of Type 2. Measurement parameters: Sample bias voltage $V=200$ mV and tunneling current $I=5$ pA in (a) and (b), $V=100$ mV and $I=20$ pA in the inset of (a), $V=200$ mV and $I=5$ pA in (i), and $V=1$ mV and $V_{ac}=10$ mV in (c), (j).

(HOMO) and the lowest unoccupied molecular orbital (LUMO), respectively. Thus, the HOMO–LUMO gap of Type 1 was approximately 3.1 eV. The spatial distributions of these electronic states are seen in the constant height dI/dV maps recorded at bias voltages of -0.6 V and 2.5 V (Figure 2b, 2c). We found that the HOMO state is located at the silole rings while the LUMO state exhibits much higher intensity at the biphenyl backbone. Similar electronic states were also observed in the 1,4-disilabenzene.^[36] Constant current dI/dV maps also show the similar bright features (Figure S9). The DFT calculated projected density of states (pDOS) of Type 1 adsorbed on a bare Au(111) surface exhibits overall similar features compared to the STS measurement (Figure 2d). In the occupied region, the contribution from the bromine atoms near -1.1 eV increases

although the absolute magnitude of pDOS contribution from all carbon atoms was greater. In the unoccupied region, increasing pDOS starting at around $+1.8$ eV coming from carbon and silicon atoms was observed, which then peaks at around $+2.1$ eV. The local density of states (LDOS) of all states between -1.5 and 2.5 eV were carefully checked, which allowed the identification of HOMO and LUMO-like orbitals of Type 1 on Au(111) (Figure 2e, 2f). Between these two regions, the pDOS of the molecule stayed mostly constant, apart from small contributions from the Si atoms (further confirming that there is hybridization between Si and Au atoms), which matches with the clean band gap observed in the experiment. Additionally, we conducted constant height dI/dV simulations, in which the bromine atoms dominate at both HOMO and LUMO energies

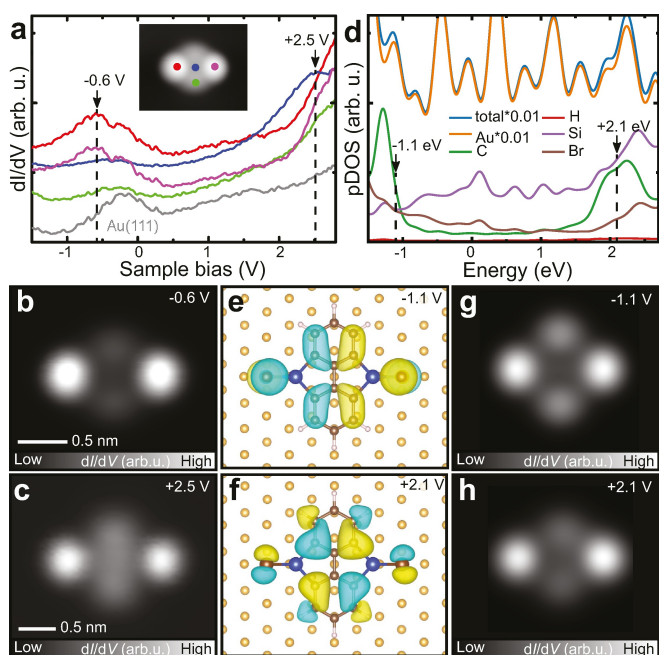


Figure 2. Electronic properties of Type 1 molecule. (a) dI/dV curves measured at the four sites of Type 1 and on the bare Au(111) surface as indicated by dots in the inset. Constant height dI/dV maps measured at bias voltages of (b) -0.6 V and (c) 2.5 V. (d) Calculated density of state of Type 1. (e–h) Calculated orbitals and simulated constant height images at -1.1 V and $+2.1$ V. Measurement parameters: $V = -0.6$ V, $V_{ac} = 10$ mV in (b). $V = 2.5$ V, $V_{ac} = 10$ mV in (c).

(Figure 2g, 2h). At the HOMO energy, the signal intensity above the biphenyl backbone was larger at the top and bottom edges of the biphenyl whereas the contrast was more equally distributed at the LUMO energy, and a similar observation was also seen in the experiment (Figure 2b, 2c).

In contrast to **1**, **2** has two Br atoms at the *peri* position at each side. We deposited **2** on Au(111) partially covered with the AuSi_x layer at room temperature, subsequently annealing at 470 K for 5 min. Similar to the reaction with **1**, the AuSi_x layer disappears, and consequently the bare Au(111) surface was restored. We observed the formation of one-dimensional structures on the surface (Figure 3a). The close-up view shows that the shape of the product differs from those of organometallic chains^[25,44] and N=5 armchair GNRs synthesized with **2** alone on a clean Au(111) surface (inset of Figure 3a).^[45] The bright dots in the one-dimensional structures are located at periodic sites with a gap of 1.10 ± 0.01 nm while the apparent STM heights vary (Figure 3b). The large corrugation amplitude of the bright dots prevented high-resolution imaging in constant height mode because the CO molecule on the tip apex was often detached due to excessive interactions. Thus, we attempted to resolve only the molecular backbone by setting a narrow scan area as indicated by a square in Figure 3b. Although it is not clear in the dI/dV map (Figure 3c), we could see the perylene backbone, which was formed via debrominative homo-coupling of **2** (Figure 3c, d). Since the longitudinal axis of the perylene is 0.7 nm in length, the bright dot results in a gap of 0.4 nm. Given the fact that the length of a C–Si bond is in a range of 0.18 – 0.20 nm,^[36,42,46,47] we assigned a

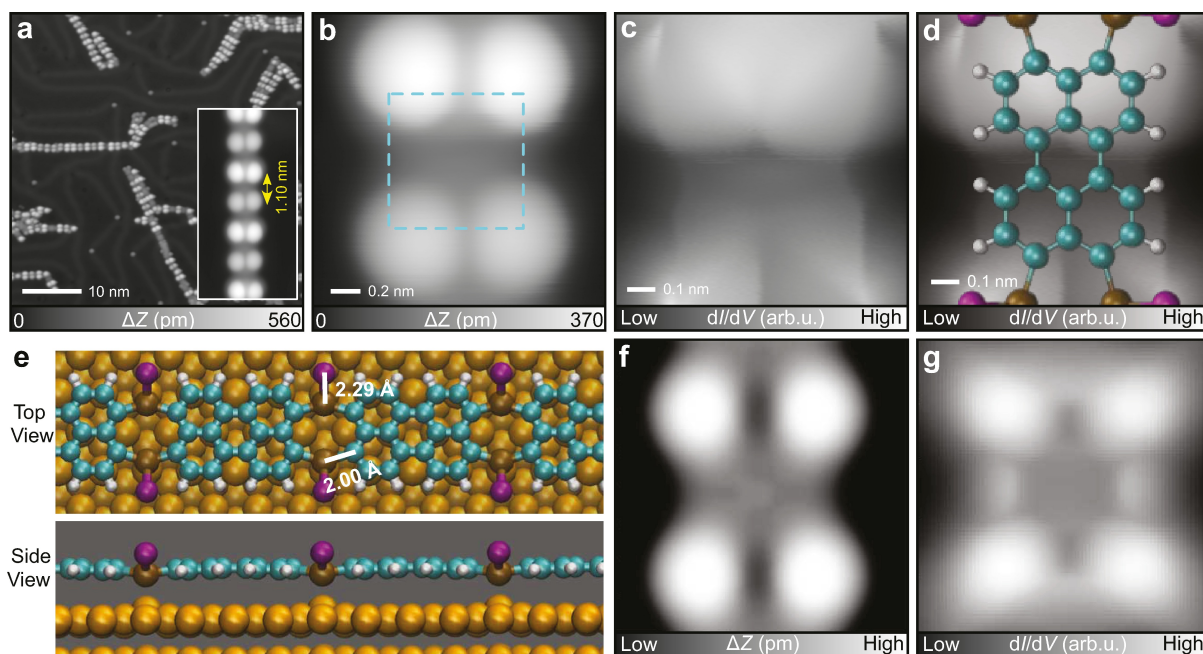


Figure 3. Synthesis of eight-membered sila-cyclic rings bridged nanoribbon structures. (a) Large-scale STM topography of the surface after annealing at 470 K for 5 min. Inset shows the STM topography of individual nanoribbon. (b) Close-up view of one unit in a nanoribbon. (c) High-resolution constant height dI/dV map of the area indicated by dashed square in (b). (d) Chemical model superimposed on (c). (e) Optimized structure of the nanoribbon. (f, g) Simulated constant current STM image, simulated bond-resolved dI/dV map. Measurement parameters: $V = 200$ mV and $I = 2$ pA in (a). $V = 200$ mV and $I = 5$ pA in (b). $V = 1$ mV, $V_{ac} = 10$ mV in (c).

C–Si–C bond as the linker. The incorporated Si atom was passivated by one Br atom, appearing as the bright dot in the STM topography.^[36] Since two dots were seen between the perylene units, two sets of C–Si–C bridges should exist, indicating formation of a $C_6Si_2Br_2$ ring, the so-called eight-membered sila-cyclic ring bridged nanoribbon structures (Figure 3e). To verify our assignment of the structure, we conducted DFT calculations of the ribbon structure adsorbed on bare Au(111). Again, we saw bonding between the silicon and gold atoms and similar orientation of the Si–Br bond compared to Type 1 (Figure 3e), and STM simulations confirmed that the bright dots can be attributed to the bromine atoms (Figure 3f, 3g). We constructed the DFT unit cell to include two perylene and Si–Br pairs to investigate the varying brightness of bromine atoms, but the optimized structure is mostly planar, and the silicon atoms adsorb on equivalent top sites resulting in no difference in brightness. The elongated C–Si bonds (0.2 nm) were attributed to the slightly increased lattice constant of the nanoribbon to achieve commensurability with the substrate. To investigate the reason for the apparent alternation we constrained one pair of bromine atoms to relax 0.02 nm lower than the adjacent pair and the simulated STM image of this structure showed alternating brightness (Figure 4j). Therefore, we assign the contrast difference to different silicon adsorption sites affecting the bromine height.

To investigate the electronic properties of eight-membered sila-cyclic ring bridged nanoribbon, we performed STS measurements focusing on a particular case where the ribbon exhibits periodically undulating brightness. Compared with the result on the bare Au(111) surface (grey curve), we found three distinct peaks at -0.6 V, 1.9 V and 2.5 V, which were measured above three different sites in the nanoribbon (Figure 4a). The two bright dots with different contrasts exhibit distinct empty states at 1.9 V and 2.5 V, which may be related to their adsorption heights because the substrate polarization effect enhanced by a strong adsorption shifts the empty state towards the Fermi level.^[48,49] The occupied state was visible at -0.6 V only above the dots with the higher adsorption height in nanoribbon. Nevertheless, the band gap of this nanoribbon is 2.5 eV. The STM topographies and the simultaneously recorded dI/dV maps obtained at bias voltages of -0.6 V, 1.9 V and 2.5 V show that the three electronic states mainly distribute on the sites of eight-membered rings (Figure 4b–g). The calculated pDOS of the nanoribbon rapidly increased in the unoccupied region, with energies larger than $+1.9$ eV peaking at approximately $+2.5$ eV (Figure 4h). In the occupied region there was a brief increase in pDOS between -0.5 eV and -1.0 eV. Simulated constant current STM images were mostly dominated by the lobes located at bromine atom sites, appearing larger with positive energies (Figure 4i, 4k, 4m). The orbital structures at -0.6 eV, $+1.9$ eV and $+2.5$ eV corresponded with the STM images, showing that the lobes were the result of bromine atoms orienting upwards from the substrate (Figure 4j, 4l, 4n).

In addition to the C_6Si_2 rings, we also found other sila-cyclic rings. Figure 5a shows an example, which has a planar

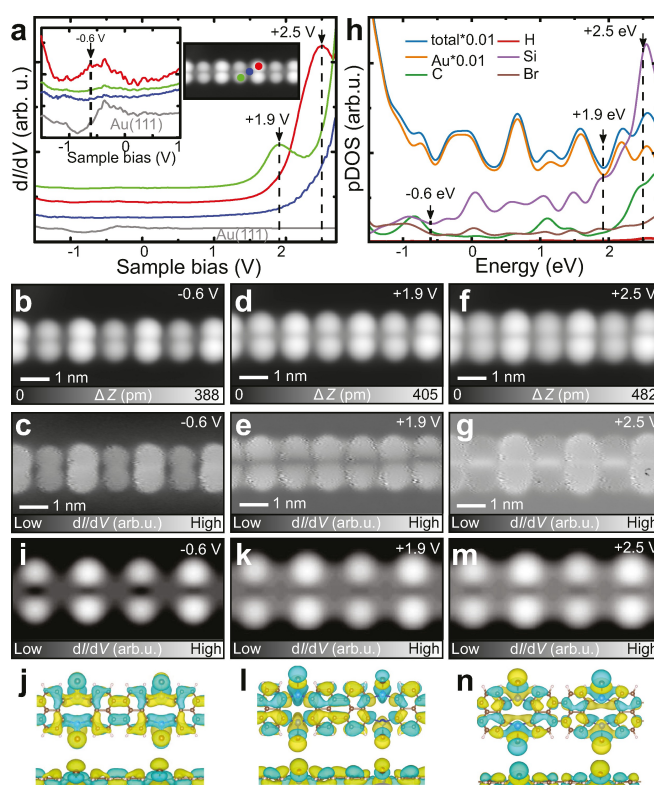


Figure 4. Electronic properties of C_6Si_2 sila-cyclic ring bridged nanoribbon. (a) dI/dV curves recorded on the nanoribbon (inset of (a)) and the bare Au(111) substrate. (b–g) Constant current STM topographies and the corresponding dI/dV maps measured at sample bias voltages of -0.6 V, 1.9 V and 2.5 V, respectively. (h) Calculated density of states of the eight-membered sila-cyclic ring bridged nanoribbon and (i–n) the corresponding constant current STM simulations and orbitals of occupied and unoccupied states in top and side views. Measurement parameters: $V = -0.6$ V, $I = 150$ pA in (b). $V = -0.6$ V, $I = 150$ pA, $V_{ac} = 10$ mV in (c). $V = 1.9$ V, $I = 220$ pA in (d). $V = 1.9$ V, $I = 220$ pA, $V_{ac} = 10$ mV in (e). $V = 2.5$ V, $I = 220$ pA in (f). $V = 2.5$ V, $I = 220$ pA, $V_{ac} = 10$ mV in (g).

segment as indicated by an arrow (also see Figure S10). The close-up view indicates that the segment has two faint dots (inset of Figure 5a). The corresponding bond-resolved constant height dI/dV map (Figure 5b) and Laplace filtered image (Figure S11) revealed the detailed structure as two silole rings incorporated into a nanoribbon segment (Figure 5c). The C_5Si ring was most probably formed through a sequential process involving debromination, C–C coupling, dehydrogenation, and C–Si coupling of the nanoribbon segments and Si atoms (see Figure S12). Figure 5d shows another type of the planar segment, in which two dots attached to the edges of nanoribbon as indicated by an arrow. The constant height dI/dV map (Figure 5e) and Laplace filtered image (Figure S13) indicate the formation of a quaterylene unit incorporated by two five-membered sila-cyclic rings (C_4Si) (Figure 5f). This structure was most probably generated through sequential coupling reactions of the nanoribbon segments and Si atoms (Figure S14). Finally, flat nanoribbon structures with dark lines, running across the longitudinal axis, were found (Figure 5g). A close-up

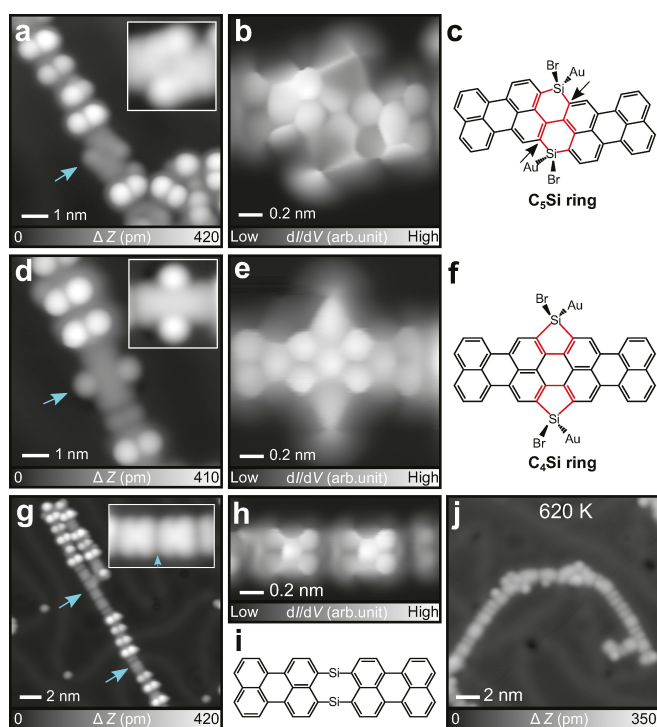


Figure 5. Various sila-cyclic rings incorporated in nanoribbon structures. (a) STM topography of one nanoribbon. Inset shows the segment indicated by an arrow in (a). (b) High-resolution constant height dI/dV map of the segment, and (c) the corresponding chemical structure. (d) STM topography of another nanoribbon. Inset shows the segment indicated by arrow in (d). (e) High-resolution constant height dI/dV map of the segment, and (f) the corresponding chemical structure. (g) STM topography of two nanoribbon structures. Inset shows the segment with dark line. (h) High-resolution constant height dI/dV map of the segment. (i) Chemical model of debromination in $C_6Si_2Br_2$ moieties between two perylene. (j) STM topography of the sample after annealing at 620 K for 5 min. Measurement parameters: $V=200$ mV and $I=2$ pA in (a), $V=200$ mV and $I=5$ pA in (d). $V=200$ mV and $I=4$ pA in (g), and $V=1$ mV and $V_{ac}=10$ mV in (b), (e), (h).

view shows one nanoribbon segment separated by dark line as indicated by an arrow (inset of Figure 5g). The bond-resolved STM image (Figure 5h) and the corresponding Laplace filtered image (Figure S15) revealed that each segment corresponds to the perylene unit. However, we found that the structure around the dark line cannot be resolved by constant height dI/dV mapping. Given the fact that the individual Si atom is strongly adsorbed to the Au(111) surface,^[36] the dark lines should relate to the presence of the Si atom (Figure 5i). Since there was no bright dot in the STM topography and no characteristic contrast in the dI/dV map, it is likely that Br atoms have already desorbed from the Si atom in the product. Thus, we deduce that the perylene units were linked by a C_6Si_2 ring. In fact, high-temperature annealing at 620 K induced removal of the bright spots from the nanoribbon structures (Figure 5j, Figure S16).

Conclusion

We synthesized two five-membered sila-cyclic rings (C_4Si) incorporated molecule Type 1 and eight-membered rings (C_6Si_2) bridged nanoribbon structures on Au(111) by reacting Si atoms with molecules **1** and **2**, respectively. Their chemical structures were revealed by bond-resolved STM and DFT calculations. A HOMO–LUMO gap of 3.1 eV was determined for Type 1 molecules (further comparative calculations were shown in Figure S17) and a band gap of 2.5 eV was assigned to eight-membered rings bridged nanoribbon by STS measurements. This research demonstrates the robustness of a synthetic strategy to obtain low-dimensional Si incorporated nanostructures by direct on-surface coupling. We foresee that this method has a potential to be extended to the synthesis nanostructure incorporating heavier elements, such as germanium, allowing for even more flexibility over the resulting electronic structure.

Acknowledgements

This work was supported in part by Japan Society for the Promotion of Science (JSPS) KAKENHI Grant Number 22H00285. Kewei Sun acknowledges the supporting of ICYS project. The authors acknowledge funding from the Academy of Finland (project no. 346824). A.S.F. was supported by the World Premier International Research Center Initiative (WPI), MEXT, Japan. L.K. acknowledges funding from the Finnish Cultural Foundation. The authors acknowledge the computational resources provided by the Aalto Science-IT project and CSC, Helsinki. The authors acknowledge Ondřej Krejčí for valuable discussion.

Conflict of Interest

The authors declare no conflict of interest.

Data Availability Statement

The data that support the findings of this study are available from the corresponding author upon reasonable request.

Keywords: on-surface synthesis · sila-cyclic rings · nanoribbon structures · scanning tunneling microscopy/spectroscopy · density functional theory

- [1] C. Friedel, J. M. Crafts, *Liebigs Ann. Chem.* **1863**, 127, 28–32.
- [2] R. Muller, *J. Chem. Educ.* **1965**, 42, 41–47.
- [3] A. G. Brook, *J. Am. Chem. Soc.* **1958**, 80, 1886–1889.
- [4] P. A. Di Giorgio, L. H. Sommer, F. C. Whitmore, *J. Am. Chem. Soc.* **1948**, 70, 3512–3514.
- [5] A. G. Brook, F. Abdesaken, B. Gutekunst, G. Gutekunst, R. K. Kallury, *J. C. S. Chem. Comm.* **1981**, 191–192.
- [6] K. Rühlmann, V. Hagen, K. Schiller, *Z. Chem.* **1967**, 7, 353–354.
- [7] N. Tokitoh, *Acc. Chem. Res.* **2004**, 37, 86–9.

- [8] S. Okumura, F. Sun, N. Ishida, M. Murakami, *J. Am. Chem. Soc.* **2017**, *139*, 12414–12417.
- [9] W. Zhao, F. Gao, D. Zhao, *Angew. Chem. Int. Ed.* **2018**, *57*, 6329–6332.
- [10] K. Kubota, C. L. Hamblett, X. Wang, J. L. Leighton, *Tetrahedron* **2006**, *62*, 11397–11401.
- [11] P. R. Carlson, A. S. Burns, E. A. Shimizu, S. Wang, S. D. Rychnovsky, *Org. Lett.* **2021**, *23*, 2183–2188.
- [12] M. Birot, J. P. Pilot, J. Dunogues, *Chem. Rev.* **1995**, *95*, 1443–1477.
- [13] Q. Mu, J. Chen, C. Xia, L. Xu, *Coord. Chem. Rev.* **2018**, *374*, 93–113.
- [14] K. Tamao, M. Uchida, T. Izumizawa, K. Furukawa, S. Yamaguchi, *J. Am. Chem. Soc.* **1996**, *118*, 11974–11975.
- [15] M. Uchida, T. Izumizawa, T. Nakano, S. Yamaguchi, K. Tamao, K. Furukawa, *Chem. Mater.* **2001**, *13*, 2680–2683.
- [16] J. Luo, Z. Xie, J. W. Y. Lam, L. Cheng, H. Chen, C. Qiu, H. S. Kwok, X. Zhan, Y. Liu, D. Zhu, B. Z. Tang, *Chem. Commun.* **2001**, 1740–1741.
- [17] Z. Zhao, B. He, B. Z. Tang, *Chem. Sci.* **2015**, *6*, 5347–5365.
- [18] L. Grill, M. Dyer, L. Lafferentz, M. Persson, M. V. Peters, S. Hecht, *Nat. Nanotechnol.* **2007**, *2*, 687–691.
- [19] J. Cai, P. Ruffieux, R. Jaafar, M. Bieri, T. Braun, S. Blankenburg, M. Muoth, A. P. Seitsonen, M. Saleh, X. Feng, K. Müllen, R. Fasel, *Nature* **2010**, *466*, 470–473.
- [20] J. I. Urgel, S. Mishra, H. Hayashi, J. Wilhelm, C. A. Pignedoli, M. D. Di Giovannantonio, R. Widmer, M. Yamashita, N. Hieda, P. Ruffieux, H. Yamada, R. Fasel, *Nat. Commun.* **2019**, *10*, 861.
- [21] L. Grossmann, B. T. King, S. Reichmaier, N. Hartmann, J. Rosen, W. M. Heckl, J. Björk, M. Lackinger, *Nat. Chem.* **2021**, *13*, 730–736.
- [22] S. Hla, L. Bartels, G. Meyer, K. Rieder, *Phys. Rev. Lett.* **2000**, *85*, 2777–2780.
- [23] K. Kaiser, L. M. Scriven, F. Schulz, P. Gawel, L. Gross, H. L. Anderson, *Science* **2019**, *365*, 1299–1301.
- [24] L. Grill, S. Hecht, *Nat. Chem.* **2020**, *12*, 115–130.
- [25] W. Wang, X. Shi, S. Wang, M. A. Van Hove, N. Lin, *J. Am. Chem. Soc.* **2011**, *133*, 13264–13267.
- [26] Y.-Q. Zhang, N. Kepčija, M. Kleinschrodt, K. Diller, S. Fischer, A. C. Papageorgiou, F. Allegretti, J. Björk, S. Klyatskaya, F. Klappenberger, M. Ruben, J. V. Barth, *Nat. Commun.* **2012**, *3*, 1286.
- [27] H.-Y. Gao, H. Wagner, D. Zhong, J.-H. Franke, A. Studer, H. Fuchs, *Angew. Chem. Int. Ed.* **2013**, *52*, 4024–4028.
- [28] S. Kawai, O. Krejčí, A. S. Foster, R. Pawlak, F. Xu, L. Peng, A. Orita, E. Meyer, *ACS Nano* **2018**, *12*, 8791–8797.
- [29] Q. Sun, C. Zhang, Z. Li, H. Kong, Q. Tan, A. Hu, W. Xu, *J. Am. Chem. Soc.* **2013**, *135*, 8448–8451.
- [30] B. Schuler, S. Fatayer, F. Mohn, N. Moll, N. Pavliček, G. Meyer, D. P. Peña, L. Gross, *Nat. Chem.* **2016**, *8*, 220–224.
- [31] V. K. Kanuru, G. Kyriakou, S. K. Beaumont, A. C. Papageorgiou, D. J. Watson, R. M. Lambert, *J. Am. Chem. Soc.* **2010**, *132*, 8081–8086.
- [32] T. Wang, J. Huang, H. Lv, Q. Fan, L. Feng, Z. Tao, H. Ju, X. Wu, S. L. Tait, J. Zhu, *J. Am. Chem. Soc.* **2018**, *140*, 13421–13428.
- [33] K. Sun, K. Sagisaka, L. Peng, H. Watanabe, F. Xu, R. Pawlak, E. Meyer, Y. Okuda, A. Orita, S. Kawai, *Angew. Chem. Int. Ed.* **2021**, *60*, 19598–19603.
- [34] D. Zhong, J. H. Franke, S. K. Podiyanchari, T. Blomker, H. Zhang, G. Kehr, G. Erker, H. Fuchs, L. Chi, *Science* **2011**, *334*, 213–216.
- [35] K. Sun, A. Chen, M. Liu, H. Zhang, R. Duan, P. Ji, L. Li, Q. Li, C. Li, D. Zhong, K. Müllen, L. Chi, *J. Am. Chem. Soc.* **2018**, *140*, 4820–4825.
- [36] K. Sun, O. J. Silveira, Y. Ma, Y. Hasegawa, M. Matsumoto, S. Kera, O. Krejčí, A. S. Foster, S. Kawai, *Nat. Chem.* **2023**, *15*, 136–142.
- [37] O. Deniz, C. Sánchez-Sánchez, T. Dumschlaff, X. Feng, A. Narita, K. Müllen, N. Kharche, V. Meunier, R. Fasel, P. Ruffieux, *Nano Lett.* **2017**, *17*, 2197–2203.
- [38] K. Sun, S. Kawai, *Phys. Chem. Chem. Phys.* **2021**, *23*, 5455–5459.
- [39] K. Sun, T. Nishiuchi, K. Sahara, T. Kubo, A. S. Foster, S. Kawai, *J. Phys. Chem. C* **2020**, *124*, 19675–19680.
- [40] L. Gross, F. Mohn, N. Moll, P. Liljeroth, G. Meyer, *Science* **2009**, *325*, 1110–1114.
- [41] R. Temirov, S. Soubatch, O. Neucheva, A. C. Lassise, F. S. Tautz, *New J. Phys.* **2008**, *10*, 053012.
- [42] P. Pyykkö, *J. Phys. Chem. A* **2015**, *119*, 2326–2337.
- [43] S. Kawai, K. Takahashi, S. Ito, R. Pawlak, T. Meier, P. Spijker, F. F. Canova, J. Tracey, K. Nozaki, A. S. Foster, E. Meyer, *ACS Nano* **2017**, *11*, 8122–8130.
- [44] K. Sun, X. Li, L. Chen, H. Zhang, L. Chi, *J. Phys. Chem. C* **2020**, *124*, 11422–11427.
- [45] H. Zhang, H. Lin, K. Sun, L. Chen, Y. Zagranyski, N. Aghdassi, S. Duhm, Q. Li, D. Zhong, Y. Li, K. Müllen, H. Fuchs, L. Chi, *J. Am. Chem. Soc.* **2015**, *137*, 4022–4025.
- [46] W. F. Sheehan, V. Schomaker, *J. Am. Chem. Soc.* **1952**, *74*, 3956–3957.
- [47] S. Goel, X. Luo, R. L. Reuben, *Appl. Phys. Lett.* **2012**, *100*, 231902.
- [48] J. B. Neaton, M. S. Hybertsen, S. G. Louie, *Phys. Rev. Lett.* **2006**, *97*, 216405.
- [49] K. S. Thygesen, A. Rubio, *Phys. Rev. Lett.* **2009**, *102*, 046802.

Manuscript received: January 16, 2024

Accepted manuscript online: February 28, 2024

Version of record online: March 15, 2024